A γ-Secretase Independent Role for Presenilin in Calcium Homeostasis Impacts Mitochondrial Function and Morphology in *Caenorhabditis elegans*

Shaarika Sarasija and Kenneth R. Norman[1]
Center for Cell Biology and Cancer Research, Albany Medical College, Albany, New York 12208

ABSTRACT Mutations in the presenilin (PSEN) encoding genes (*PSEN1* and *PSEN2*) occur in most early onset familial Alzheimer's Disease. Despite the identification of the involvement of PSEN in Alzheimer's Disease (AD) ~20 years ago, the underlying role of PSEN in AD is not fully understood. To gain insight into the biological function of PSEN, we investigated the role of the PSEN homolog SEL-12 in *Caenorhabditis elegans*. Using genetic, cell biological, and pharmacological approaches, we demonstrate that mutations in *sel-12* result in defects in calcium homeostasis, leading to mitochondrial dysfunction. Moreover, consistent with mammalian PSEN, we provide evidence that SEL-12 has a critical role in mediating endoplasmic reticulum (ER) calcium release. Furthermore, we found that in SEL-12-deficient animals, calcium transfer from the ER to the mitochondria leads to fragmentation of the mitochondria and mitochondrial dysfunction. Additionally, we show that the impact that SEL-12 has on mitochondrial function is independent of its role in Notch signaling, γ-secretase proteolytic activity, and amyloid plaques. Our results reveal a critical role for PSEN in mediating mitochondrial function by regulating calcium transfer from the ER to the mitochondria.

KEYWORDS *Caenorhabditis elegans*; calcium; endoplasmic reticulum; mitochondria; presenilin

MITOCHONDRIA are highly dynamic organelles that are responsible for a myriad of functions including ATP production, generation and metabolism of reactive oxygen species (ROS), and apoptosis (Detmer and Chan 2007). Thus cells, in particular muscle cells and neurons due to their high-energy demands, are extremely reliant on mitochondrial function. Mitochondria also play a critical role in calcium homeostasis by acting as a calcium buffer. Calcium, in turn, regulates mitochondrial morphology, activity, and movement. The relevance of mitochondria is highlighted by the fact that many neurodegenerative diseases, such as Parkinson's and Alzheimer's Disease (AD) are characterized by abnormal mitochondrial activity and morphology (Cali *et al.* 2012).

Mutations in the genes encoding presenilins (PSENs), *PSEN1* and *PSEN2*, are the most common cause of early onset familial Alzheimer's Disease (FAD). PSENs are ~50-kDa multipass transmembrane proteins that reside predominantly on the endoplasmic reticulum (ER) (Bezprozvanny and Mattson 2008) and have been shown to be enriched in an ER subcompartment that is in contact with mitochondria (Area-Gomez *et al.* 2009). Although altered PSEN function has been known to have a role in AD for 20 years (Sherrington *et al.* 1995), the functional consequences of mutations in PSENs are controversial and not understood. The prevailing model for the pathogenesis of AD is the "amyloid hypothesis," which states that an increase in β amyloid (Aβ) 42 peptide is the major cause of neuronal degradation in AD (Hardy and Selkoe 2002); support for this hypothesis stems from the accumulation of amyloid plaques in the brains of AD patients (Hardy 2006). In addition to the "amyloid hypothesis," there is a large body of work that suggests that dysregulation of intracellular calcium has a central role in the pathogenesis of AD. Indeed, several laboratories have shown that FAD mutant PSENs affect store-operated calcium influx by increasing the activity or expression of ER calcium channels [*e.g.*, ryanodine receptors (RYR) (Chan *et al.* 2000), inositol 1,4,5 trisphosphate receptors (IP_3R) (Leissring *et al.* 1999; Stutzmann *et al.* 2004; Cheung *et al.* 2008), or sarco-endoplasmic

doi: 10.1534/genetics.115.182808
Manuscript received September 13, 2015; accepted for publication October 19, 2015; published Early Online October 21, 2015.
Supporting information is available online at www.genetics.org/lookup/suppl/doi:10.1534/genetics.115.182808/-/DC1.
[1]Corresponding author: 47 New Scotland Ave., MC-165, Center for Cell Biology and Cancer Research, Albany Medical College, Albany, NY 12208. E-mail: normank@mail.amc.edu

reticulum calcium ATPases (SERCA) (Green *et al.* 2008a)] and that PSENs themselves have been shown to act as standalone ER calcium leak channels (Tu *et al.* 2006; Bandara *et al.* 2013). Moreover, PSENs are a crucial component of the γ-secretase complex, an intramembranous multi-subunit protease. In addition to the cleavage of amyloid precursor protein (APP) into Aβ peptides, γ-secretase has also been implicated in the cleavage of several other transmembrane proteins, including Notch and APP-like proteins (Beel and Sanders 2008).

In this study, we set out to understand the role of PSEN in the regulation of calcium homeostasis and mitochondrial function in the model system *Caenorhabditis elegans*. The *C. elegans* PSEN family comprises the three genes *hop-1*, *sel-12*, and *spe-4* (Levitan and Greenwald 1995; Li and Greenwald 1997; Arduengo *et al.* 1998). Although *hop-1* and *sel-12* are widely expressed, including in muscle and neurons (Levitan and Greenwald 1998), the more distantly related *spe-4* is exclusively expressed in the male germline (Arduengo *et al.* 1998). From our studies, we demonstrate that mutations in *sel-12* cause increased calcium signaling and mitochondrial fragmentation and dysfunction. Moreover, we find that the mitochondrial defects observed in *sel-12* mutants are independent of γ-secretase activity and are caused by ER-mediated calcium transfer to the mitochondria. Furthermore, we find evidence that the structural and functional defects in mitochondria of *sel-12* mutants render them susceptible to oxidative stress and reduce their life span.

Materials and Methods

C. elegans strains and genetics

C. elegans were grown on OP50-seeded NGM plates at 20° except where noted. Animals were synchronized for all experiments by bleaching plates containing gravid worms, and the progeny were rocked in M9 buffer for <48 hr. The synchronized L1s were then allowed to grow on NGM plates seeded with OP50 until the stage required for the experiments was reached. For experiments that required sterilization, age-synchronized L4s were moved to 0.5 mg/ml 5-fluorour-aci1-2'-deoxyribose (FUDR) (Sigma) containing NGM plates seeded with OP50. The following strains were used in this study: wild type (N2), *sel-12 (ar131*, *ty11 and ok2078)*, *hop-1 (ar179)*, *ccIs4251*, *zxIs3*, *unc-68(r1162)*, *crt-1(jh101)*, *mcu-1(tm6026)*, *egl-19(tak5)*, *egl-19(n2368)*, *akEx885*, *takIs13*, *glp-1(e2141)*, *lin-12(ok2215)*, *syIs243*, *stEx30*, and *adIs2122*.

Levamisole assay

Briefly, 15–20 age-synchronized L4 or young adult worms from each strain were picked onto individual 0.5-mM levamisole-containing NGM plates by someone other than an assay executioner. At each time point, worms were gently prodded on their head with a platinum pick three times, and in the event of a lack of response, they were marked as paralyzed and eliminated from the assay. Levamisole assay was observed for >70 min. Six replicate assays were done.

Channelrhodopsin analysis

We used the *C. elegans* strain *zxIs3* [*Punc-47*::ChR2(H134R)::YFP + *lin-15(+)*] that expresses channelrhodopsin (ChR2) in their GABAergic motor neurons (Liewald *et al.* 2008). This optogenetic study was performed as previously described (Liewald *et al.* 2008; Fry *et al.* 2014), and the percentage elongation of the animals was calculated using the equation below.

$$\%\ \text{relaxation} = \frac{(\textit{length upon blue light illumination} - \textit{initial length prior to blue light illumination})}{\textit{initial length prior to blue light illumination}} \times 100\%$$

DNA constructs and transgenesis

The *Pmyo-3*::R-GECO1 construct was assembled by cloning PCR-amplified R-GECO1 into the vector containing the *myo-3* promoter pPD95.86 (a gift from Andrew Fire, Addgene). Using standard procedures, these constructs, along with pJM23 [*lin-15(+)*], were injected into *lin-15(n765ts)* animals (Jin *et al.* 1999). Transgenic progeny were identified by body-wall or pharyngeal muscle fluorescence and *lin-15* mutant rescue. Stable integrated lines (*takIs13*) were generated with γ-irradiation using standard procedures (Jin *et al.* 1999; Spooner *et al.* 2012). A full-length *sel-12* cDNA that contains a 3′ SL2::TagRFP cassette was generated by Genscript. To make the *Pmyo-3*::*sel-12*::SL2::TagRFP construct, this synthesized *sel-12* cDNA was placed into a vector containing the *myo-3* promoter pPD95.86 (Addgene). To make the *Prab-3*::*sel-12*::SL2::TagRFP construct, the *myo-3* promoter was replaced with a PCR-amplified *rab-3*, pan-neuronal promoter (Mahoney *et al.* 2008). Using standard procedures, these constructs along with the coinjection marker *Pttx-3*::GFP were injected into N2 animals. Transgenic progeny were identified by appropriate tissue fluorescence.

Calcium imaging

The basal calcium levels in the body-wall muscle of animals were analyzed by expressing R-GECO1 under the *myo-3* promoter (Moerman and Fire 1997). Briefly, five age-synchronized sterilized young adults were mounted on a 2.5% agarose in M9 pad and immobilized using Polybead Polystyrene 0.10 μm microspheres (Polysciences). The animals were imaged at 10× magnification using an inverted Zeiss AxioObserver microscope equipped with an Andor Clara CCD camera. For each genotype, we analyzed 50 animals. A Wacom Bamboo tablet and stylus were used to draw freehand selections around each immobilized animal for each image, and their fluorescence intensity was measured using Metamorph software. Relative R-GECO1 fluorescence in each strain compared to wild-type R-GECO1 fluorescence. Protein levels of R-GECO1 in each strain were used to normalize the fluorescence intensity. Protein levels of R-GECO1 were detected using Western blot analysis. Briefly, a large plate of FUDR-sterilized, synchronized day 1 adult worms from each strain were freeze-cracked in RIPA buffer, sonicated, and spun down at 4° to collect supernatant. This supernatant was then used for Western analysis using previously established methods (Kelsh *et al.* 2014). R-GECO1 levels were probed using a

DsRed Polyclonal Antibody (Clontech catalog no. 632496) antibody, and protein loading was verified using an Anti-Actin Antibody, clone C4 antibody (EMD Millipore).

To analyze calcium transients, we utilized the same technique but imaged the worms, one worm/ agar pad/slide, under 63× oil while focusing on a single muscle cell for 50 sec. The fluorescence intensity of the R-GECO1 in this muscle cell was measured over this time period and adjusted for photobleaching. A calcium transient was scored as observed when F/F0 was >5%.

Mitochondrial morphology analysis

Body-wall mitochondrial structure was analyzed using the *ccIs4251* strain [*Pmyo-3*::GFP(NLS)::LacZ (PSAK2) + *Pmyo-3*::GFP (PSAK4) + *dpy-20(+)*], which targets GFP to the matrix of the body-wall muscle mitochondria and nucleus and the *syIs243* strain [*Pmyo-3*::TOM20::mRFP + *unc-119*(+) + pBS SK+], which targets monomeric red fluorescent protein (mRFP) to the outer mitochondrial membrane. These strains were crossed into various genotypes to determine mitochondrial structure. Age-synchronized day 1 adults (nongravid) were immobilized, and their mitochondrial structure was imaged under the 63× oil objective on a Zeiss AxioObserver microscope equipped with a Andor Clara CCD camera. Images were compiled, and the mitochondria were scored as linear, intermediate, or fragmented (Lu *et al.* 2011) under blinded conditions. Neuronal mitochondria were assessed similarly using *akEx885* (*Pnmr-1*::Su9::GFP; kindly provided by A. V. Maricq).

MitoTracker Red CMXRos (Life Technologies) and tetramethylrhodamine ethyl ester (TMRE) were used to determine the structural and functional integrity of the body-wall muscle mitochondria in various *C. elegans* strains. Briefly, age-synchronized worms (L4s for Mitotracker and young adults for TMRE) were stained with either 1nμg/ml of Mitotracker or 200 nM of TMRE in M9 with OP50 for 6 hr with shaking at 20°. Worms were then washed four times with M9. Mitotracker and TMRE-stained animals were destained overnight or for 1 hr, respectively. Worms were imaged as day 1 adults as per the protocol described above.

Inhibition of γ-secretase activity

Unseeded NGM plates were coated with 100 μl of 100 μM Compound E (Calbiochem), a γ-secretase inhibitor, and were then seeded with OP50 the next day. Synchronized L1 staged animals were grown on these plates, and day 1 adults were used for analysis (Francis *et al.* 2002). γ-Secretase inhibition was confirmed by the *glp-1*-like sterility observed in the *hop-1(ar179)* mutants that were grown on the Compound E-containing plates.

RNA interference

Age-synchronized L1 animals were allowed to grow to day 1 adults on RNA interference (RNAi) plates seeded with empty vector, *itr-1*, or *drp-1* RNAi-containing bacteria.

Drug treatments

Thapsigargin (Abcam) (Xu *et al.* 2001), mito-TEMPO (Sigma) (Johnson *et al.* 2012), and cyclosporine A (Sigma) (Giacomotto *et al.* 2013) were dissolved in DMSO and added to the NGM media (cooled to 55°) to the appropriate final concentrations, and animals were grown on these plates as previously described.

2′,7′-dichlorodihydrofluorescein diacetate assay

Three replicate 2′,7′-dichlorodihydrofluorescein diacetate (H_2DCF-DA) assays (Life Technologies) were used to measure ROS levels in wild type, *sel-12(ar131)*, *sel-12(ty11)*, and *sel-12(ok2078)* animals. Animals grown on 100-mm NGM plates were washed three times with M9 to remove OP50. Then the animals were washed once in PBS and resuspended in 100 μl of PBS followed by freeze thawing and 10 sec of sonication. After spinning down the sample at 20,000 × *g* for 10 min at 4°, the protein concentration was determined using a BCA protein assay (Pierce). Twenty-five micrograms of the protein was used for each strain, the samples were incubated with H_2DCF-DA at 37° for 4 hr, and a Flex Station 3 Reader (Molecular Devices) was used to measure fluorescence intensity.

Paraquat assay

Sensitivity to paraquat (Aldrich) was analyzed as previously described (Han *et al.* 2012). Briefly, 50 animals per strain were placed in tubes containing 100 μl of 0, 50, 100, or 150 mM paraquat in M9 buffer and incubated at 20° for 24 hr. Subsequently, the animals were moved to an NGM plate and their survival was observed. Animals were marked as dead if they showed no response to three gentle pats from a platinum pick. These experiments were repeated three times.

Statistical analysis

GraphPad Prism software was used for statistical analysis. Student's *t*-test was used for comparing two samples, and one-way ANOVA with Bonferroni posttest was used while making multiple comparisons. The chi-square test was used to compare the mitochondrial structural distribution between strains.

Results

sel-12 mutants are hypersensitive to levamisole

To gain insight into the physiological role that PSEN has in *C. elegans*, we turned to a simple and widely used pharmacological assay using levamisole, an acetylcholine receptor agonist that promotes progressive paralysis by hypercontraction of the body-wall muscle. We examined whether the null mutations *sel-12(ty11)* and *sel-12(ok2078)* or the missense mutation *sel-12(ar131)*, which is a conserved change identified in FAD patients (Tedde *et al.* 2003), causes a different behavioral response to levamisole compared to wild-type animals. Upon exposure to levamisole for 70 min, only 24.4% of *sel-12(ar131)*, 16.3% of *sel-12(ty11)*, and 14.8% of *sel-12(ok2078)* animals were moving compared to 58.5% of wild-type animals (Figure 1A). Since previous

studies have implicated PSENs in the regulation of calcium (Leissring *et al.* 1999; Chan *et al.* 2000; Green *et al.* 2008b; Brunello *et al.* 2009; Chakroborty *et al.* 2009), we next investigated whether reducing calcium signaling in *sel-12* mutants could suppress the hypersensitivity of *sel-12* mutants to levamisole. Accordingly, we introduced *unc-68(r1162)*, a RYR null mutation, into the *sel-12* mutant background and tested levamisole sensitivity. Strikingly, introduction of the *unc-68* mutation into the *sel-12* mutant background suppressed the elevated sensitivity of *sel-12* mutants to levamisole. When exposed to levamisole, 79.1% of *unc-68*; *sel-12(ar131)* and 82.4% of *unc-68*; *sel-12(ty11)* mutants are motile unlike *sel-12(ar131)* and *sel-12(ty11)* mutants, which are 24.4 or 16.3% motile, respectively (Figure 1B). These results taken together suggest that elevated sensitivity of *sel-12* mutants to levamisole may result from elevated calcium signaling.

sel-12 mutants are defective in GABAergic inhibitory motor neuron-induced muscle relaxation and have reduced motility

We reasoned that if *sel-12* mutants have elevated calcium signaling in the body-wall muscle, their muscle should be less responsive to inhibitory neuronal signaling. To investigate this possibility, we used an optogenetic approach utilizing *zxIs3* animals that express ChR2 in their GABAergic inhibitory motor neurons (Liewald *et al.* 2008). In *zxIs3* animals, blue light stimulation of ChR2 will cause the depolarization of GABAergic inhibitory motor neurons, resulting in the relaxation of body-wall muscles and measurable elongation of the animal (Liewald *et al.* 2008; Fry *et al.* 2014). If *sel-12* animals have elevated cytoplasmic calcium levels, we predict that *sel-12* mutants will not elongate to the same extent as wild-type animals. Freely crawling *zxIs3* and *zxIs3*; *sel-12(ty11)* animals were illuminated with blue light, and their percentage changes in body length were measured. Upon stimulation, wild-type animals extend their body length 3.7% while *sel-12* mutants show a significant decrease in their ability to relax and extend 1.5% (Figure 1C). Consistent with this defect in muscle relaxation, *sel-12* mutants also show reduced locomotive abilities in both crawling (Supporting Information, Figure S1A) and swimming assays (Figure S1B). These data demonstrate that *sel-12* mutants have an inability to elongate normally upon muscle inhibition and have reduced locomotion, which is consistent with *sel-12* mutants having elevated calcium signaling.

SEL-12 is required for maintaining cellular calcium homeostasis

PSEN mutations have been reported to be detrimental to calcium homeostasis in various *in vitro* and *in vivo* models (Leissring *et al.* 1999; Chan *et al.* 2000; Smith *et al.* 2005; Green *et al.* 2008b; Brunello *et al.* 2009; Chakroborty *et al.* 2009). Consistent with these observations, our data suggest that there is elevated calcium signaling in the body-wall muscle of *sel-12* mutants. To directly measure calcium levels in *sel-12* mutants, we generated transgenic animals that express R-GECO1, a red-shifted genetically encoded calcium indicator (GECI) (Zhao *et al.* 2011), in the cytosol of body-wall muscle. We evaluated calcium levels in the body-wall muscle based on fluorescence intensity of R-GECO1 in *sel-12(ty11)* mutants. These values were normalized to the R-GECO1 protein content relative to wild-type animals in each strain using Western blot analysis. The relative fluorescence intensity of R-GECO1 with respect to relative protein content in *sel-12* mutants is 48.4% higher than in wild-type animals (Figure 2A and Figure S2). Additionally, we examined calcium transients in immobilized intact animals by measuring the fluorescence intensity of R-GECO1 in wild-type and *sel-12(ty11)* mutant animals. Calcium transients coincide with muscle contraction and are dependent on RYR function (Liu *et al.* 2011). *sel-12* mutants have 3.2 transients/50 sec whereas wild-type animals show only 1.2 transient/50 sec (Figure 2, B and C). The significantly higher fluorescence intensity and increased number of calcium transients indicates that loss of SEL-12 function results in elevated calcium signaling.

Abnormal mitochondrial morphology is observed in sel-12 mutants

When cytoplasmic calcium levels within cells increase, mitochondria will facilitate the uptake of calcium. To investigate whether the elevated calcium signaling observed in *sel-12* mutants leads to an alteration in mitochondrial organization, we examined the morphology of mitochondria in the body-wall muscle of *sel-12* mutants. We utilized a transgenic strain, *ccIs4251*, which expresses green fluorescent protein (GFP) that localizes to the nucleus and the mitochondrial matrix (Fire *et al.* 1998). Examination of wild-type animals reveals that the majority of mitochondria in the body-wall muscle are organized into a parallel and linear network (Figure 3, A and B). However, the mitochondria in *sel-12* mutants are disorganized and display a fragmented appearance (Figure 3, A and B). While we observed only 2.9% fragmentation in the mitochondrial network in wild-type animals, the fragmentation of mitochondria in *sel-12(ar131)*, *sel-12(ty11)*, and *sel-12(ok2078)* mutants is 34.5, 55.6, and 47.2%, respectively (Figure 3, A and B). We analyzed the organization of body-wall muscle myosin in *sel-12* mutants to rule out the possibility of widespread structural damage in the muscle using the strain *stEx30*, which expresses GFP-labeled body-wall-muscle-specific myosin. Strikingly, the myosin organization in *sel-12* mutants is indistinguishable from that of wild-type animals (Figure S3A), indicating that the mitochondrial morphology defects observed in the *sel-12* mutants is not the result of comprehensive muscle structural defects. We also examined an additional transgenic strain with mRFP fused to TOMM-20, an outer mitochondrial membrane protein in the body-wall muscle and observed similar mitochondrial fragmentation in *sel-12* mutants (Figure S3B). To determine whether SEL-12 has a cell-autonomous role in maintaining mitochondrial morphology, we expressed wild-type *sel-12* under a body-wall-muscle-specific promoter (*Pmyo-3*). Expression of *sel-12* in the body-wall muscle is successful in

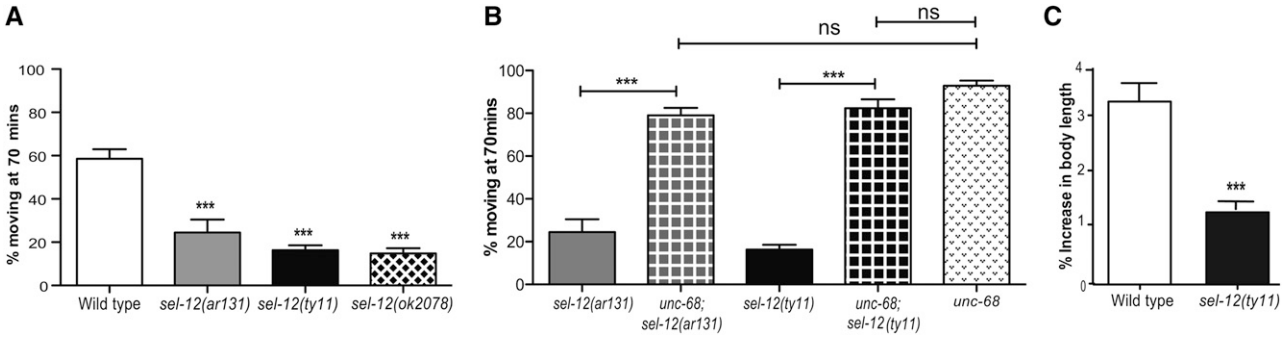

Figure 1 *sel-12* mutants have hyper-excitable muscle. (A) *sel-12* mutants are hypersensitive to 0.5 mM of levamisole. (B) Rescue of *sel-12* mutant hypersensitivity to 0.5 mM of levamisole by *unc-68* mutant background. For A and B, data are displayed as mean ± SEM (***$P < 0.001$ using one-way ANOVA). (C) *sel-12* mutants elongate significantly less than wild-type animals upon GABAergic motor neuron activation. $n = 30$ animals per genotype. Data are displayed as mean ± SEM, and all comparisons have been made to wild type unless otherwise indicated (***$P < 0.001$ using two-tailed *T*-tests).

rescuing the mitochondrial fragmentation in *sel-12(ty11)* animals (Figure 3B). However, the expression of wild-type *sel-12* under a pan-neuronal promoter (*Prab-3*) does not result in rescue of the mitochondrial defects observed in *sel-12(ty11)* animals (Figure 3B). These data indicate that SEL-12 works via a cell-autonomous mechanism to regulate mitochondrial morphology. Of note, although not as severe as observed in *sel-12* mutants, overexpression of *sel-12* by the body-wall-muscle-specific or pan-neuronal promoter in wild-type animals leads to an increase in mitochondrial morphology defects (Figure 3B), suggesting that overexpression of *sel-12* in the muscle can lead to mitochondrial disorganization and that overexpression of *sel-12* in the nervous system can lead to non-cell-autonomous defects. These data indicate that *sel-12* needs to be tightly regulated for normal mitochondrial morphology.

Since mutations in human PSENs lead to neuronal dysfunction and loss, we next investigated the impact of *sel-12* mutations on neuronal mitochondria. We examined mitochondrial morphology in the PVC interneurons, which are two interneurons that are located in the tail region and are easily and reliably identified. Similar to the mitochondrial morphology observed in the body-wall muscle, we find that 48.4 and 26.3% of PVC neuronal mitochondria in *sel-12(ty11)* and *sel-12(ar131)* mutants are fragmented compared to only 12.7% observed in the wild-type animals (Figure 3, C and D). Taken together, these data suggest that *sel-12* mutations lead to an alteration of mitochondrial morphology in both the body-wall muscle and neurons.

SEL-12-deficient mitochondrial structural defects are Notch and γ-secretase-independent

PSENs are essential for Notch signaling as it forms part of the γ-secretase complex, a protease that cleaves within the membrane-spanning region of Notch to promote Notch signaling (Struhl and Greenwald 1999). The *C. elegans* genome encodes two Notch family members, LIN-12 and GLP-1 (Priess 2005; Greenwald 2012). To determine whether the mitochondrial defects observed in *sel-12* mutants are caused by the downregulation of Notch signaling, we analyzed mitochondria in *glp-1* and *lin-12* mutants. Strikingly, the mitochondrial structure in both Notch mutants is similar to those of wild-type animals with *glp-1* and *lin-12* mutants exhibiting comparable proportions of linear, intermediate, and fragmented mitochondria to wild-type animals (Figure 3, E and F). Since Notch-dependent signaling does not appear to have a role in the SEL-12-deficient mitochondrial phenotype, we next investigated whether γ-secretase activity is required to maintain normal mitochondrial morphology. We used a well-characterized γ-secretase inhibitor called Compound E, which has been previously shown to inhibit all SEL-12-mediated γ-secretase activity but not the γ-secretase activity of HOP-1 (Francis *et al.* 2002). To completely abolish all γ-secretase activity, we grew *hop-1(ar179)* null mutants on plates containing Compound E and examined their mitochondria. The mitochondria of γ-secretase-inhibited animals are indistinguishable from wild-type animals (Figure 3G), suggesting that the mitochondrial defects observed in the *sel-12* mutants are not mediated by the lack of γ-secretase activity. Furthermore, *hop-1(ar179);sel-12(ty11)* double-mutant animals show mitochondrial morphology similar to *sel-12(ty11)* single-mutant animals, suggesting that HOP-1, unlike SEL-12, does not influence mitochondrial structure (Figure 3H).

Elevated cytoplasmic calcium levels alone are not sufficient to cause mitochondrial fragmentation as observed in sel-12 mutants

To investigate the cause of mitochondrial fragmentation in *sel-12* mutants, we hypothesized that the high cytoplasmic calcium levels and more frequent calcium transients observed in *sel-12* mutants are responsible for the mitochondrial morphology disruption. To test this hypothesis, we utilized a reduction of function (*rof*) mutation in the gene encoding the L-type voltage-gated calcium channel, *egl-19*, which is critical for muscle contraction (Lee *et al.* 1997; Spooner *et al.* 2012). We generated *egl-19(rof)*; *sel-12(ty11)* double mutants. Using our GECI strain, we found that the *egl-19(rof)*; *sel-12* double mutants have cytoplasmic calcium levels that are significantly reduced from *sel-12* mutants and similar to those of

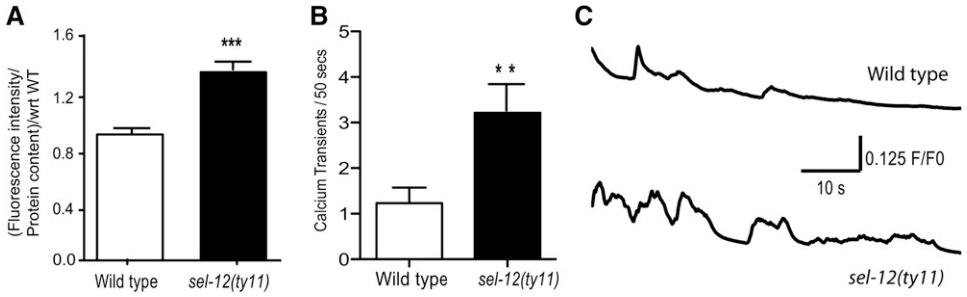

Figure 2 *sel-12* mutants have aberrant calcium homeostasis. (A) Basal cytosolic calcium level is significantly higher in *sel-12* mutants compared to wild-type animals. Data are displayed as mean relative intensity of R-GECO1 in wild-type and *sel-12* animals normalized to relative R-GECO1 protein concentration ± SEM, and all comparisons have been made to wild type unless otherwise indicated (***$P < 0.001$ using two-tailed T-tests). (B) Number of calcium transients per 50 sec observed in each strain ($n = 9$ per strain) (**$P < 0.01$ using two-tailed *t*-tests). (C) Representative traces of calcium transients observed in immobilized animals.

wild-type animals (Figure 4A and Figure S2). Next, we examined mitochondrial morphology in the double mutants. Consistent with our hypothesis, the mitochondrial morphology in *egl-19(rof)*; *sel-12* double mutants is improved compared to *sel-12* mutants, with the former having 46.4% of mitochondria in the linear form while *sel-12* mutants have only 10.2% in the linear form. Similarly, the introduction of the *egl-19(rof)* mutation into *sel-12* mutants decreases the amount of mitochondrial fragmentation observed in *sel-12* mutants from 55.6 to 20.2% (Figure 4B). Despite having cytoplasmic calcium levels similar to wild type, the *egl-19(rof)*; *sel-12* double mutants do not have wild-type mitochondria. These data suggest that, while reducing cytoplasmic calcium levels in *sel-12* mutants can improve mitochondrial morphology, it does not explain the extent of damage observed in *sel-12* mutant animals. We next investigated whether high cytoplasmic calcium levels are sufficient to cause mitochondrial fragmentation by examining the mitochondrial structure in *egl-19* gain of function (*gof*) mutants (Lee *et al.* 1997). First, using our GECI, we determined that the cytoplasmic calcium levels in *egl-19(gof)* mutants are ~10-fold higher than in wild-type animals (Figure 4C and Figure S2). While *egl-19(gof)* mutants do show significant mitochondrial morphology defects, they did not show mitochondrial defects to the same extent as *sel-12* mutants did (Figure 4D), suggesting that increased cytoplasmic calcium alone is not sufficient to explain the mitochondrial phenotype seen in *sel-12* mutants.

Reduction of calcium release from the ER can rescue sel-12 mutant mitochondrial defects

PSENs are found predominantly in the ER membrane and have been implicated in calcium release from the ER and mutant forms or loss of PSEN has been shown to augment ER calcium release (Leissring *et al.* 1999; Chan *et al.* 2000; Smith *et al.* 2005; Chakroborty *et al.* 2009). EGL-19 voltage-gated calcium channels are located in the plasma membrane and are separated from the mitochondria by the myofilament lattice, which, due to the abundance of calcium-binding proteins, acts as a calcium buffer (Altun 2009; Kim *et al.* 2009) (Figure 5A). However, the more proximal location of the ER to the mitochondria indicates that ER calcium release may impact mitochondria more than calcium entry from the more distally positioned EGL-19 channels (Figure 5A). To investigate whether exacerbated ER calcium release can result in mitochondrial fragmentation, we grew wild-type animals carrying the mitochondrial GFP marker (*ccIs4251*) on NGM plates containing 3 μg/ml of thapsigargin. Thapsigargin is a SERCA pump inhibitor that blocks ER calcium uptake and induces calcium release via IP_3Rs, thereby increasing the calcium release from the ER and local calcium concentration (Takemura *et al.* 1989; Xu *et al.* 2001). Wild-type animals grown on thapsigargin exhibit significant fragmentation compared to vehicle-treated animals, suggesting that excessive ER-calcium release leads to the fragmentation of mitochondria similar to what is observed in *sel-12* mutants (Figure 5B).

To further investigate the impact of ER calcium release on mitochondrial morphology in *sel-12* mutants, we used four different approaches. First, we investigated the effect of RNAi knockdown of the ITR-1/IP_3R (to inhibit ER calcium release) in *sel-12(ar131)*, *sel-12(ty11)*, and wild-type animals. Compared to *sel-12(ty11)* and *sel-12(ar131)* animals grown on control RNAi, *itr-1(RNAi)*; *sel-12(ty11)* and *itr-1(RNAi)*; *sel-12(ar131)* animals show improved mitochondrial structure with significantly increased amounts of linear and decreased amounts of fragmented mitochondria (Figure S4A). Second, we introduced a RYR null mutation *unc-68(r1162)* into *sel-12(ty11)* mutants to eliminate the contribution of RYR-mediated calcium release from the ER. Interestingly, the *unc-68* single mutants show a higher level of mitochondrial fragmentation than what is observed in wild-type animals (Figure S4A). Nevertheless, from our examination of *unc-68*; *sel-12* double mutants, we find a significant improvement of mitochondrial morphology compared to *sel-12(ty11)* mutants alone (Figure S4A). Third, since genetic or RNAi ablation of *unc-68* or *itr-1* does not fully rescue the mitochondrial morphology defects observed in *sel-12* mutants (Figure S4A), we used RNAi to knockdown ITR-1/IP_3R in the *unc-68(r1162)*; *sel-12(ty11)* double mutant. Compared to *sel-12(ty11)* animals grown on control RNAi, *itr-1(RNAi)*; *unc-68(r1162)*; *sel-12(ty11)* animals show improved mitochondrial structure with linear mitochondria increasing to 65.2 from 20.9% (Figure 5C). Similarly, the amount of fragmented mitochondria observed in *sel-12(ty11)* is reduced from 43.8 to 12.1% in *itr-1(RNAi)*; *unc-68(r1162)*; *sel-12(ty11)* animals (Figure 5C). When compared to *itr*-1 RNAi-treated *unc-68(r1162)*

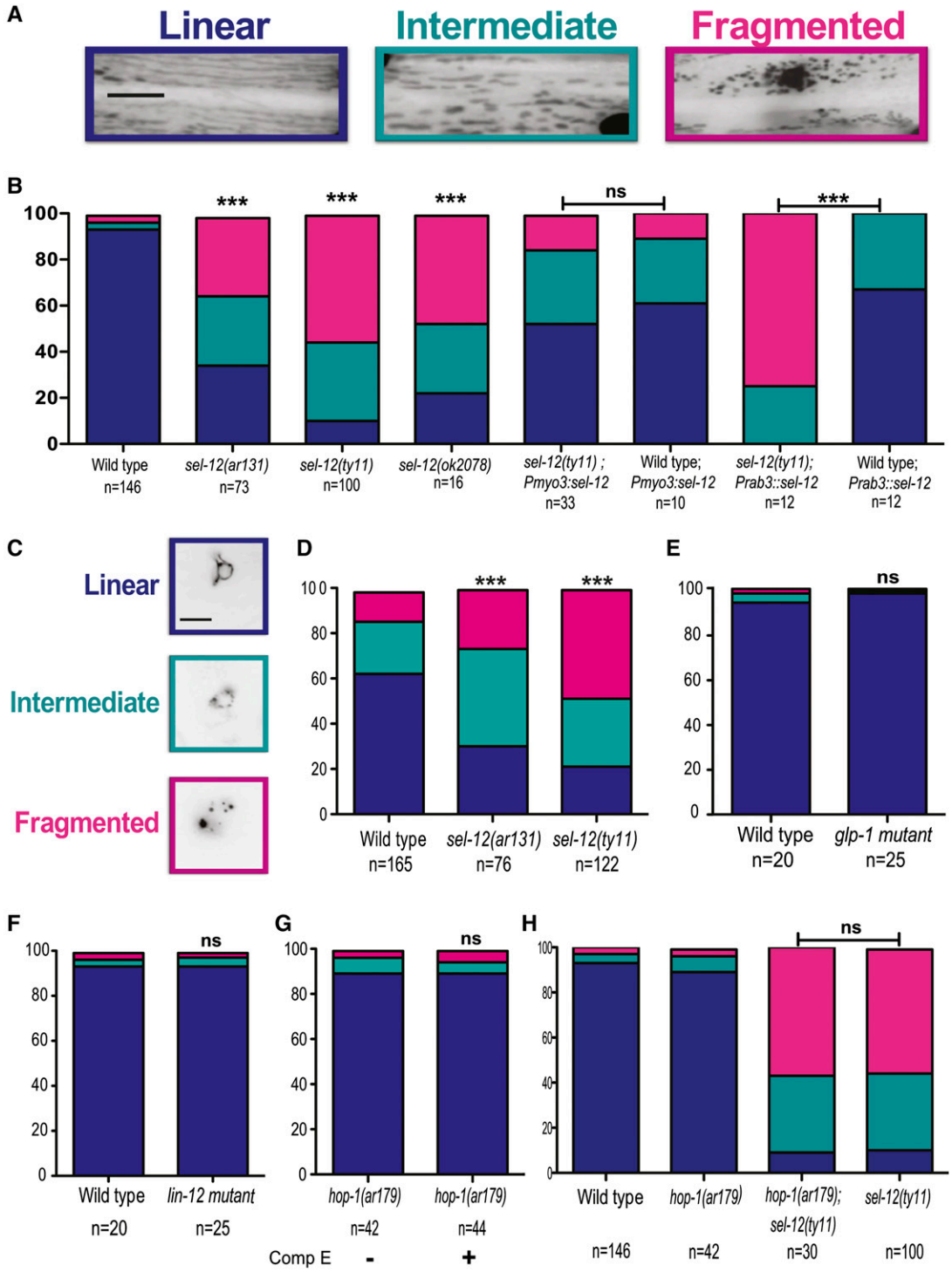

Figure 3 *sel-12* mutants have mitochondrial morphology defects. (A) Representative images of the mitochondrial morphologies observed in the body-wall muscle. (B) Quantification of body-wall muscle mitochondrial morphology in wild-type and *sel-12* animals. (C) Representative images of the mitochondrial morphologies observed in the PVC neurons. (D) Quantification of PVC neuronal mitochondrial morphology in wild-type and *sel-12* animals. (E) Quantification of body-wall muscle mitochondrial morphology in wild-type and *glp*-1 animals grown at 25°. (F) Quantification of body-wall muscle mitochondrial morphology in wild-type and *lin-12* animals. (G) Quantification of body-wall muscle mitochondrial morphology in *hop-1* mutants grown on Compound E. (H) Quantification of body-wall muscle mitochondrial morphology in wild-type, *hop-1*, *hop-1;sel-12(ty11)*, and *sel-12(ty11)* mutants. For A, B, and E–H, analysis was done using transgenic animals expressing mito::GFP in body-wall muscle cells (*ccIs4251*). For C and D, analysis was done using transgenic animals expressing mito::GFP in PVC neurons (*akEx885*). Blue, cyan, and pink represent the percentage of animals displaying linear, intermediate, and fragmented mitochondrial morphology, respectively. *n* = number of animals imaged per genotype. All comparisons have been made to wild type unless otherwise indicated, and statistical significance was tested using the chi-square test ("ns" indicates $P > 0.05$, *** $P < 0.001$). Bar, 10 μm.

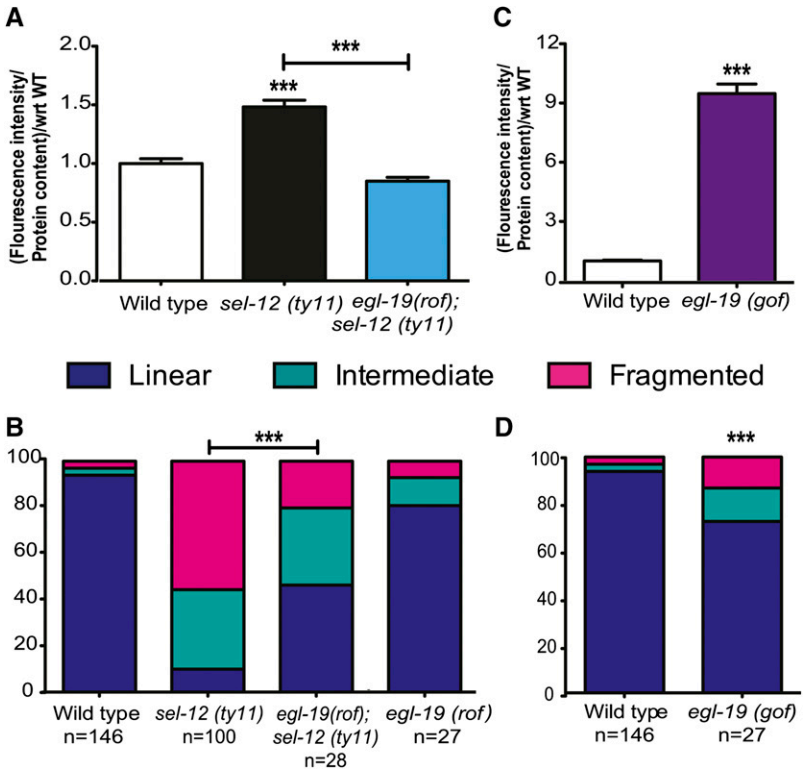

Figure 4 Elevated cytoplasmic calcium levels are not sufficient to cause the mitochondrial morphology defects observed in *sel-12* mutants. (A) Basal calcium level in wild-type, *sel-12*, and *egl-19(rof);sel-12* animals. (B) Quantification of body-wall muscle mitochondrial morphology in wild-type, *sel-12*, *egl-19(rof);sel-12*, and *egl-19(rof)* animals. (C) Basal calcium level in wild-type and *egl-19(gof)* animals. (D) Quantification of body-wall muscle mitochondrial morphology in wild-type and *egl-19(gof)* animals. In A, data are displayed as mean ± SEM (***$P < 0.001$ using the one-way ANOVA), and all comparisons have been made to wild type unless otherwise indicated. In C, data are displayed as mean ± SEM (***$P < 0.001$ using two-tailed *t*-tests). In B and D, analysis was done using transgenic animals expressing mito::GFP in body-wall muscle cells (*ccIs4251*). *n* = number of animals imaged per genotype, and statistical significance was tested using the chi-square test (***$P < 0.001$). Bar, 10 μm.

animals, *itr-1(RNAi)*; *unc-68(r1162)*; *sel-12(ty11)* animals have similar mitochondrial morphology that is not significantly different, indicating full rescue (Figure 5C). Finally, we sought to reduce ER calcium levels by genetic removal of calreticulin, a critical ER calcium-buffering protein required for normal release of ER calcium (Michalak *et al.* 1999). We introduced a null calreticulin mutation, *crt-1(jh101)*, into *sel-12(ty11)* mutants and investigated mitochondrial morphology. Accordingly, reduction of ER calcium results in a robust increase in linear mitochondria; we observed 63.3% linear mitochondria in *crt-1*; *sel-12(ty11)* double mutants compared to the 10.2% linear mitochondria in *sel-12(ty11)* mutants (Figure 5D). Similarly, there is a steep decline in mitochondrial fragmentation from 55.6% in *sel-12(ty11)* to 17.5% in *crt-1;sel-12(ty11)* animals (Figure 5D). Together, these data strongly indicate that reduction of calcium release from the ER in *sel-12* mutants can restore mitochondrial morphology and indicate that ER calcium release is critical in causing the mitochondrial morphology defects observed in *sel-12* mutants.

Decreasing calcium uptake into the mitochondrial matrix reduces sel-12 mutant mitochondrial defects

Since mitochondria act as a calcium buffer, this prompted us to investigate whether mitochondrial uptake of calcium in *sel-12* mutants mediates the mitochondrial morphology defects observed in *sel-12* mutants. Mitochondrial calcium uptake is handled by the conserved mitochondrial calcium uniporter (MCU), a highly selective calcium transporter that is activated when there is a localized increase in calcium concentration (Csordas *et al.* 2010). To this end, we employed null *mcu-1* mutants, which have been previously shown to reduce mitochondrial calcium uptake and buffering (Xu and Chisholm 2014). We generated *mcu-1*; *sel-12(ty11)* double mutants and examined their mitochondria. We found that, unlike *sel-12* mutants where 10.2% of mitochondria exist in linear structures, the *mcu-1*; *sel-12* double mutants have 42.7% of their mitochondria appear linear (Figure 6A). Furthermore, the amount of mitochondrial fragmentation is reduced from 55.6% in *sel-12* mutants to 21.2% in *mcu-1*; *sel-12* double mutants (Figure 6A). Although the rescue of mitochondrial structural defects is highly significant, it is not complete. This is not unexpected since basal levels of mitochondrial calcium are still detected in MCU knockout mice and in *mcu-1* null animals despite the impairment of rapid calcium uptake (Pan *et al.* 2013; Xu and Chisholm 2014). These data indicate that uptake of calcium into the mitochondrial matrix is critical for the mitochondrial morphology defects observed in *sel-12* mutants.

Overloading the mitochondria with calcium can trigger the opening of the mitochondrial permeability pore (mPTP), which decreases the membrane potential and causes mitochondrial release of ROS (Brookes *et al.* 2004). To investigate whether this was the cause of mitochondrial fragmentation in the *sel-12* mutants, we treated the animals with an inhibitor of the mPTP, cyclosporine A (CysA) (Broekemeier *et al.* 1989). Treatment of *sel-12* mutants with 10 nM of CysA compared to a control treatment resulted in an increase in linear mitochondria from 13.7 to 51.0% in *sel-12* animals and a simultaneous decrease of the mitochondrial fragmentation

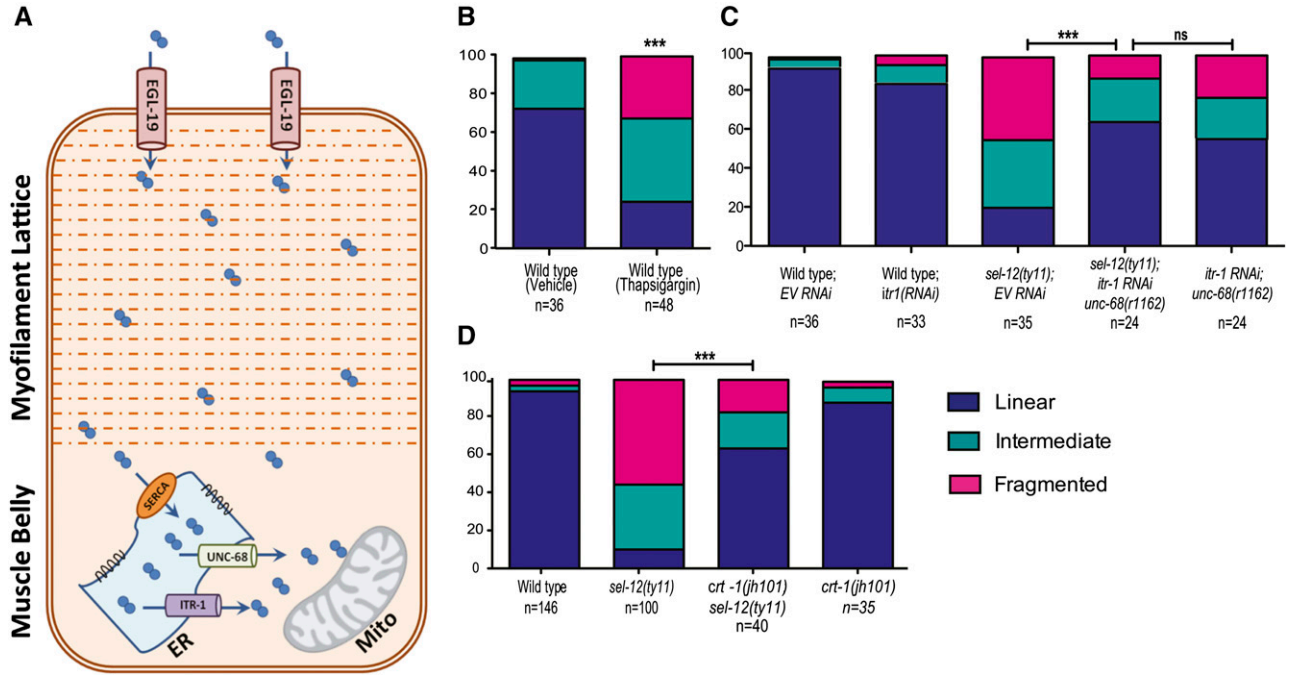

Figure 5 Decreasing ER-mediated calcium release improves mitochondrial structure in *sel-12* mutant. (A) Cartoon depicting the proximal and distal positioning of ER and EGL-19, respectively, with respect to the mitochondria in the body-wall muscle of *C. elegans*. (B) Quantification of body-wall muscle mitochondrial morphology in animals grown on NGM plates containing DMSO or 3 μg/ml of thapsigargin. (C) Quantification of body-wall muscle mitochondrial morphology in wild-type, *sel-12(ty11),unc-68;sel-12(ty11)*, and *unc-68(r1162)* animals grown on RNAi plates seeded with either empty vector (EV) or *itr-1* RNAi. (D) Quantification of body-wall muscle mitochondrial morphology in wild-type, *sel-12*, *crt-1;sel-12*, and *crt-1* animals. In B–D, analysis was done using transgenic animals expressing mito::GFP in body-wall muscle cells (*ccIs4251*). *n* = number of animals imaged per genotype. All comparisons have been made to wild type unless otherwise indicated, and statistical significance was tested using the chi-square test (***$P < 0.001$).

(Figure 6B). These data indicate that uptake of calcium into the mitochondrial matrix and the opening of the mPTP plays a critical role in the mitochondrial morphology defects observed in *sel-12* mutants.

Furthermore, ER-mediated calcium release and subsequent mitochondrial calcium uptake can impact the activity of Drp1, a mitochondrial fission protein (Cribbs and Strack 2007; Cereghetti *et al.* 2008; Xu *et al.* 2013). To determine whether DRP-1 is involved in the increased mitochondrial fragmentation observed in *sel-12* mutants, we used RNAi to knock down DRP-1 and examined mitochondrial morphology in both wild-type and *sel-12(ty11)* animals. Wild-type animals grown on *drp-1(RNAi)* exhibit a high incidence of interconnected and fused mitochondria (Figure 6, C and D), indicating successful suppression of mitochondrial fission. Markedly, *sel-12* animals grown on *drp-1(RNAi)* show reduced fragmentation and increased incidence of linear and interconnected mitochondria (Figure 6D). These data suggest that DRP-1 activity is elevated in *sel-12* mutants.

SEL-12 deficiency leads to defects in mitochondrial function

To test whether the mitochondrial fragmentation observed in *sel-12* mutants results in defective mitochondrial function, we used TMRE and MitoTracker Red CMXRos to examine the mitochondria in wild-type and *sel-12* mutants. TMRE and MitoTracker Red CMXRos are both positively charged, red fluorescent dyes that accumulate in active mitochondria because of their relative negative charge; inactive or damaged mitochondria have decreased membrane potential and will fail to sequester either dye. We found that the ratio of TMRE-labeling intensity to mitochondrial GFP intensity (from *ccIs4251*) in wild-type animals is significantly higher at 0.77 when compared to 0.25, 0.39, and 0.39 in *sel-12(ar131)*, *sel-12(ty11)*, and *sel-12(ok2078)* mutants, respectively (Figure 7A). Similarly, MitoTracker CMXRos labeling is greatly reduced in all *sel-12* mutants compared to wild-type animals (Figure S5, A and B). These data indicate that the mitochondrial membrane potential in *sel-12* mutants is reduced and suggest that mitochondrial function is abrogated.

A critical function of the mitochondria is to metabolize ROS generated by mitochondrial oxidative phosphorylation and other cellular sources (Venditti *et al.* 2013). Since we have found evidence of mitochondrial dysfunction and elevated mPTP opening in *sel-12* mutants (Figure 6B), which enhances ROS production (Brookes *et al.* 2004), we investigated ROS levels in *sel-12* mutants. ROS formation was quantified in wild-type and *sel-12* mutant animals using the membrane-permeable ROS indicator H_2DCF-DA. Consistent with mitochondrial malfunction, we find that *sel-12(ar131)*, *sel-12(ty11)*, and *sel-12(ok2078)* mutants have 1.5, 2.9, and 2.1 times as much ROS signal as wild-type animals, respectively (Figure 7B). To determine whether elevated ROS

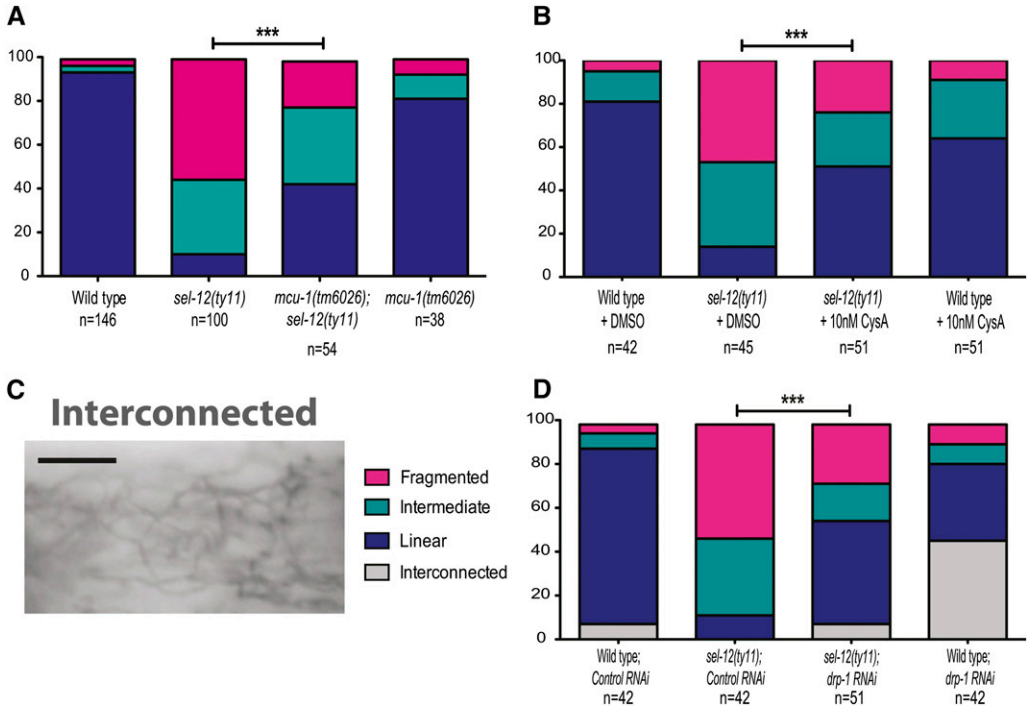

Figure 6 Mitochondrial calcium uptake is responsible for mitochondrial structural disruption in *sel-12* mutants. (A) Quantification of body-wall muscle mitochondrial morphology in wild-type, *sel-12*, *mcu-1;sel-12*, and *mcu-1* animals. (B) Quantification of body-wall muscle mitochondrial morphology in wild-type and *sel-12* animals grown on NGM plates containing DMSO or cyclosporine A. (C) Representative image of interconnected mitochondrial phenotype. (D) Quantification of body-wall muscle mitochondrial morphology in wild-type and *sel-12* animals grown on RNAi plates seeded with either empty vector (EV) or *drp-1* RNAi. Analysis was done using transgenic animals expressing mito::GFP in body-wall muscle cells (*ccIs4251*). *n* = number of animals imaged per genotype. Statistical significance was tested using the chi-square test (***$P < 0.001$). Bar, 10 μm.

levels caused mitochondrial fragmentation in *sel-12* mutants, we supplemented *sel-12* mutants with mito-TEMPO, a mitochondrial-targeted superoxide-specific antioxidant. Treatment with mito-TEMPO does not result in the rescue of mitochondrial structural defects in the *sel-12* mutants (Figure S5C). To explore the consequence of having elevated ROS levels, we exposed *sel-12* mutants to paraquat, an ROS generator that has been shown to cause toxicity dependent on endogenous ROS levels (Han *et al.* 2012). We discovered that all three *sel-12* mutants are hypersensitive to paraquat compared to wild-type animals (Figure 7C). These data suggest that mitochondrial function in *sel-12* mutants is impaired and that *sel-12* mutants are vulnerable to ROS. Furthermore, we found that the life span of *sel-12* mutants is significantly shorter compared to that of wild-type animals with all *sel-12* mutants dying 10 days prior to wild-type worms (Figure 7D). It should be noted that in a previous study *sel-12(ar131)* mutants were reported to be hypersensitive to oxidative stress, consistent with our study (Kitagawa *et al.* 2003). However, these authors also found that a null allele of *sel-12* [*sel-12(ar171)*] was long lived compared to wild-type and *sel-12(ar131)* mutants. Unlike our current study, in this previous study the *sel-12* mutants analyzed also carried an *unc-1* mutation, which encodes a stomatin-like protein that has been implicated in gap junction activity, epithelial sodium channel activity, and sensitivity to volatile anesthetics (Rajaraman and Schulder 1999; Sedensky *et al.* 2001; Chen *et al.* 2007). The influence of mutations in *unc-1* on life span and oxidative stress is unclear. Here, *sel-12(ar131)*, *sel-12(ok2078)*, and *sel-12(ty11)* all individually show defects in mitochondrial membrane potential (Figure 7A and Figure S5, *A* and *B*), elevated ROS (Figure 7B), hypersensitivity to paraquat (Figure 7C), and shortened life spans (Figure 7D). Together, these data indicate that loss of *sel-12* function leads to poor mitochondrial function and reduced organismal health.

Discussion

In this study, we provide *in vivo* evidence that SEL-12, a *C. elegans* PSEN homolog, is involved in regulating calcium homeostasis and impacts mitochondrial morphology and function. In addition, we have found that the calcium dysregulation observed in SEL-12-deficient animals arises from ER stores and that this defect leads to increased mitochondrial uptake of calcium, which drives the mitochondrial defects observed in *sel-12* mutants. Furthermore, we show that the role of SEL-12 in regulating mitochondrial function is independent of its role in γ-secretase function and that the mitochondrial defects observed in *sel-12* mutants are caused in part by the opening of the mPTP and elevated DRP-1-dependent mitochondrial fission.

Although the role of PSEN in AD progression remains unclear (Sherrington *et al.* 1995), similar to our findings, calcium dysregulation has been observed in various models of mutant PSEN function as well as tissue samples from AD patients (Ito *et al.* 1994; Leissring *et al.* 1999; Chan *et al.* 2000; Smith *et al.* 2005; Tu *et al.* 2006; Green *et al.* 2008b). Thus, calcium may have a pivotal role in AD progression. As in other animals, SEL-12 localizes predominantly to the ER (Kovacs *et al.* 1996; De Strooper *et al.* 1997; Levitan and Greenwald 1998). Furthermore, recent studies have

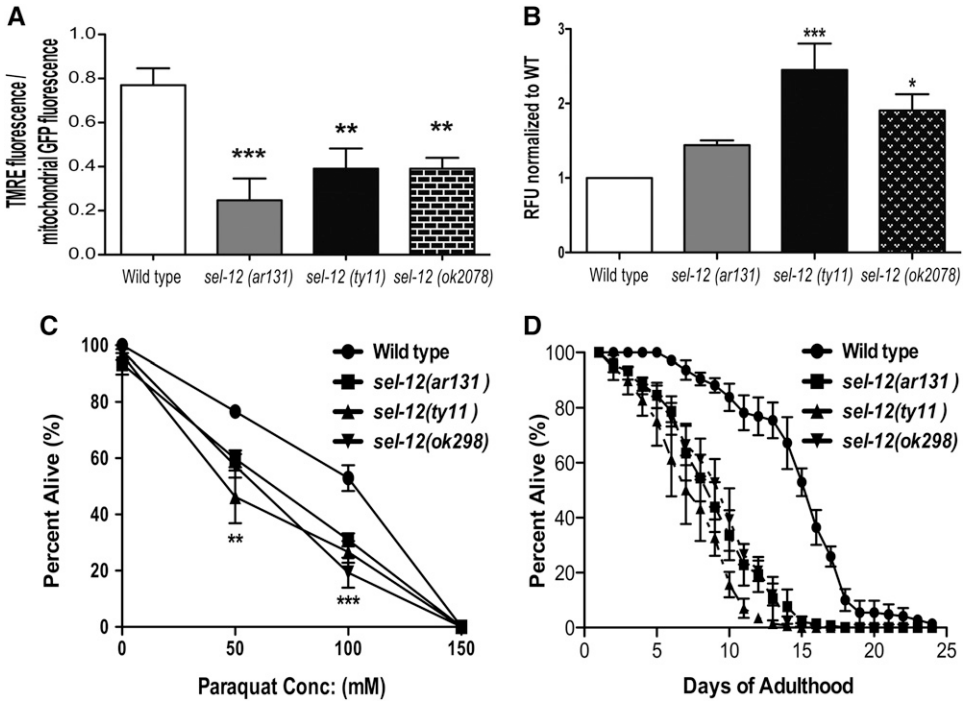

Figure 7 *sel-12* mutants have mitochondrial functional defects. (A) Quantification of body-wall muscle mitochondria staining intensity with TMRE in wild-type and *sel-12* animals. n = 30 per strain. (B) H_2DCF-DA assay measuring ROS levels relative to wild type. (C) Paraquat sensitivity in wild-type and *sel*-12 animals after 24 hr of continued exposure. Data are displayed as mean ± SEM, and all comparisons have been made to wild type ($^*P < 0.05$, $^{**}P < 0.01$, $^{***}P < 0.001$ using two-way ANOVA). In B and C, data are from three replicate assays. (D) Lifespan assay of FUDR-sterilized wild-type and *sel-12* mutant animals. n = 50 per strain. Data are from three replicate assays.

shown that PSENs are subcellularly localized on the ER to regions where ER and mitochondria contact (Area-Gomez *et al.* 2009). Moreover, ER–mitochondrial contacts are increased and ER–mitochondrial crosstalk is enhanced in PSEN1 knockout cells, in cells overexpressing the FAD mutant PSEN2, and in fibroblasts from FAD and sporadic AD patients (Zampese *et al.* 2011; Area-Gomez *et al.* 2012; Kipanyula *et al.* 2012). Thus, PSENs are critically positioned where ER and mitochondria communicate and share contents (*e.g.*, calcium, lipids, ATP). Faulty communication between the ER and mitochondria can alter the normal activity of these organelles, leading to cellular dysfunction. This is particularly underlined by our observation of the aggressive mitochondrial fragmentation brought on by thapsigargin treatment compared to the modest structural damage observed as a result of a global increase in cytoplasmic calcium levels in the *egl-19(gof)* animals. Moreover, our findings also show that reducing ER release and mitochondrial uptake of calcium corrects the mitochondrial defects observed in *sel-12* mutants. Taken together, these data indicate that SEL-12 has a critical role in mediating calcium release from the ER and, in the absence of SEL-12 function, excessive ER-mediated release of calcium causes excessive uptake into the mitochondria, resulting in loss of mitochondrial structural organization and function. Thus our current study in *C. elegans* is in agreement with the exacerbated ER–mitochondrial communication observed in AD patients as well as in PSEN knockout cells (Area-Gomez *et al.* 2012). Moreover, our data indicate that this enhanced communication between the ER and mitochondria disrupts mitochondrial function, which leads to poor organismal health.

In addition to regulating ER calcium signaling, PSENs are an essential component of the γ-secretase complex. Two well-characterized substrates for γ-secretase are Notch and APP. Inhibition of the γ-secretase blocks Notch-mediated signaling (De Strooper *et al.* 1999), thus underscoring the importance that PSEN has in promoting Notch function. Furthermore, γ-secretase-mediated cleavage of APP is crucial for generating Aβ peptides, including the toxic Aβ42 (Hardy and Selkoe 2002; Hardy 2006; Bezprozvanny and Mattson 2008). In this study, we found that inhibiting Notch function or γ-secretase activity by genetic and pharmacological approaches does not lead to mitochondrial morphology defects as observed in SEL-12-deficient animals. Thus, our study provides novel evidence that the role of SEL-12 in impacting mitochondrial function is independent of γ-secretase activity. Moreover, the *C. elegans* homolog of APP, APL-1, is incapable of forming Aβ plaques since it lacks Aβ peptide sequences and β-secretase recognition sites (Daigle and Li 1993; McColl *et al.* 2012). Furthermore, no Aβ peptides have been detected in *C. elegans* (McColl *et al.* 2012). Thus, the mitochondrial defects that we observe in SEL-12-deficient animals are not due to toxic Aβ peptides. It is noteworthy that many mouse models of AD exhibit cognitive decline well before the appearance of amyloid plaques (Lesne *et al.* 2008). Similarly in humans, plaque load does not correlate with the degree of dementia, and postmortem analyses of some AD patients with severe memory deficits have shown a lack of plaque formation (Terry *et al.* 1991). Also, neuroimaging techniques have shown extensive plaque formation in people with no cognitive impairment (Nordberg 2008; Villemagne *et al.* 2008). Furthermore, mitochondria dysfunction is highly reported in AD models and patients and may occur prior to the formation of amyloid plaques (Swerdlow *et al.* 2010; Cali *et al.* 2012; Leuner *et al.* 2012; Schon and Area-Gomez 2013; Sepulveda-Falla *et al.* 2014). While these previous studies suggest that amyloid

plaques might not be required to cause AD pathogenesis but could be a subsequent consequence of cellular (*e.g.*, mitochondria) dysfunction, they are confounded by the presence of amyloid plaques. However, our study of PSEN function in *C. elegans*, which lack Aβ peptides, provides clear evidence that the mitochondrial morphology and functional defects observed in *sel-12* mutants are mediated by ER calcium dysregulation and not by amyloid plaques.

Neurons are particularly sensitive to mitochondrial function. Indeed, postsynaptic mitochondria clear cytoplasmic calcium by direct uptake of calcium and provide ATP, which is required for calcium extrusion via plasma membrane calcium ATPases or SERCAs. Additionally, mitochondria metabolize ROS species, which can be detrimental to cellular health. In *sel-12* mutants, due to irregular calcium homeostasis, we have found evidence of mitochondrial malfunction including loss of mitochondrial membrane potential, elevated ROS, whole-animal susceptibility to ROS, and reduced life span. The generation and accumulation of ROS can lead to neuronal dysfunction and ultimately neurodegeneration. Therefore, understanding the role that PSENs have in mitochondrial function will be crucial to defining its role in AD.

Acknowledgments

We thank A. Maricq and A. Fire for reagents and P. McKeown-Longo, Y. Tang, and their lab members for reagents and support. Some nematode strains were provided by the Caenorhabditis Genetics Center, which is funded by National Institutes of Health (NIH) Office of Research Infrastructure Programs (P40 OD010440). The Alzheimer's Association (NIRG-09-132122) and NIH (GM088213) supported this work.

Literature Cited

Altun, Z. F., and D. H. Hall, 2009 Muscle system, introduction. In WormAtlas. Edited for the web by Laura A. Herndon. Last revision: May 2, 2012. DOI: 10.3908/wormatlas.1.6.

Altun, Z. F. and D. H. Hall, 2009 Muscle system, somatic muscle. In WormAtlas. Edited for the web by Laura A. Herndon. Last revision: May 31, 2013. DOI: 10.3908/wormatlas.1.7.

Arduengo, P. M., O. K. Appleberry, P. Chuang, and S. W. L'Hernault, 1998 The presenilin protein family member SPE-4 localizes to an ER/Golgi derived organelle and is required for proper cytoplasmic partitioning during Caenorhabditis elegans spermatogenesis. J. Cell Sci. 111(Pt 24): 3645–3654.

Area-Gomez, E., A. J. de Groof, I. Boldogh, T. D. Bird, G. E. Gibson *et al.*, 2009 Presenilins are enriched in endoplasmic reticulum membranes associated with mitochondria. Am. J. Pathol. 175: 1810–1816.

Area-Gomez, E., M. Del Carmen Lara Castillo, M. D. Tambini, C. Guardia-Laguarta, A. J. de Groof *et al.*, 2012 Upregulated function of mitochondria-associated ER membranes in Alzheimer disease. EMBO J. 31: 4106–4123.

Bandara, S., S. Malmersjo, and T. Meyer, 2013 Regulators of calcium homeostasis identified by inference of kinetic model parameters from live single cells perturbed by siRNA. Sci. Signal. 6: ra56.

Beel, A. J., and C. R. Sanders, 2008 Substrate specificity of gamma-secretase and other intramembrane proteases. Cell. Mol. Life Sci. 65: 1311–1334.

Bezprozvanny, I., and M. P. Mattson, 2008 Neuronal calcium mishandling and the pathogenesis of Alzheimer's disease. Trends Neurosci. 31: 454–463.

Broekemeier, K. M., M. E. Dempsey, and D. R. Pfeiffer, 1989 Cyclosporin A is a potent inhibitor of the inner membrane permeability transition in liver mitochondria. J. Biol. Chem. 264: 7826–7830.

Brookes, P. S., Y. Yoon, J. L. Robotham, M. W. Anders, and S. S. Sheu, 2004 Calcium, ATP, and ROS: a mitochondrial love-hate triangle. Am. J. Physiol. Cell Physiol. 287: C817–C833.

Brunello, L., E. Zampese, C. Florean, T. Pozzan, P. Pizzo *et al.*, 2009 Presenilin-2 dampens intracellular Ca2+ stores by increasing Ca2+ leakage and reducing Ca2+ uptake. J. Cell. Mol. Med. 13: 3358–3369.

Cali, T., D. Ottolini, and M. Brini, 2012 Mitochondrial Ca(2+) and neurodegeneration. Cell Calcium 52: 73–85.

Cereghetti, G. M., A. Stangherlin, O. Martins de Brito, C. R. Chang, C. Blackstone *et al.*, 2008 Dephosphorylation by calcineurin regulates translocation of Drp1 to mitochondria. Proc. Natl. Acad. Sci. USA 105: 15803–15808.

Chakroborty, S., I. Goussakov, M. B. Miller, and G. E. Stutzmann, 2009 Deviant ryanodine receptor-mediated calcium release resets synaptic homeostasis in presymptomatic 3xTg-AD mice. J. Neurosci. 29: 9458–9470.

Chan, S. L., M. Mayne, C. P. Holden, J. D. Geiger, and M. P. Mattson, 2000 Presenilin-1 mutations increase levels of ryanodine receptors and calcium release in PC12 cells and cortical neurons. J. Biol. Chem. 275: 18195–18200.

Chen, B., Q. Liu, Q. Ge, J. Xie, and Z. W. Wang, 2007 UNC-1 regulates gap junctions important to locomotion in C. elegans. Curr. Biol. 17: 1334–1339.

Cheung, K. H., D. Shineman, M. Muller, C. Cardenas, L. Mei *et al.*, 2008 Mechanism of Ca2+ disruption in Alzheimer's disease by presenilin regulation of InsP3 receptor channel gating. Neuron 58: 871–883.

Cribbs, J. T., and S. Strack, 2007 Reversible phosphorylation of Drp1 by cyclic AMP-dependent protein kinase and calcineurin regulates mitochondrial fission and cell death. EMBO Rep. 8: 939–944.

Csordas, G., P. Varnai, T. Golenar, S. Roy, G. Purkins *et al.*, 2010 Imaging interorganelle contacts and local calcium dynamics at the ER-mitochondrial interface. Mol. Cell 39: 121–132.

Daigle, I., and C. Li, 1993 apl-1, a Caenorhabditis elegans gene encoding a protein related to the human beta-amyloid protein precursor. Proc. Natl. Acad. Sci. USA 90: 12045–12049.

De Strooper, B., M. Beullens, B. Contreras, L. Levesque, K. Craessaerts *et al.*, 1997 Phosphorylation, subcellular localization, and membrane orientation of the Alzheimer's disease-associated presenilins. J. Biol. Chem. 272: 3590–3598.

De Strooper, B., W. Annaert, P. Cupers, P. Saftig, K. Craessaerts *et al.*, 1999 A presenilin-1-dependent gamma-secretase-like protease mediates release of Notch intracellular domain. Nature 398: 518–522.

Detmer, S. A., and D. C. Chan, 2007 Functions and dysfunctions of mitochondrial dynamics. Nat. Rev. Mol. Cell Biol. 8: 870–879.

Fire, A., S. Xu, M. K. Montgomery, S. A. Kostas, S. E. Driver *et al.*, 1998 Potent and specific genetic interference by double-stranded RNA in Caenorhabditis elegans. Nature 391: 806–811.

Francis, R., G. McGrath, J. Zhang, D. A. Ruddy, M. Sym *et al.*, 2002 aph-1 and pen-2 are required for Notch pathway signaling, gamma-secretase cleavage of betaAPP, and presenilin protein accumulation. Dev. Cell 3: 85–97.

Fry, A. L., J. T. Laboy, and K. R. Norman, 2014 VAV-1 acts in a single interneuron to inhibit motor circuit activity in Caenorhabditis elegans. Nat. Commun. 5: 5579.

Giacomotto, J., N. Brouilly, L. Walter, M. C. Mariol, J. Berger *et al.*, 2013 Chemical genetics unveils a key role of mitochondrial dynamics, cytochrome c release and IP3R activity in muscular dystrophy. Hum. Mol. Genet. 22: 4562–4578.

Green, K. N., A. Demuro, Y. Akbari, B. D. Hitt, I. F. Smith *et al.*, 2008a SERCA pump activity is physiologically regulated by presenilin and regulates amyloid beta production. J. Gen. Physiol. 132: i1.

Green, K. N., A. Demuro, Y. Akbari, B. D. Hitt, I. F. Smith *et al.*, 2008b SERCA pump activity is physiologically regulated by presenilin and regulates amyloid beta production. J. Cell Biol. 181: 1107–1116.

Greenwald, I., 2012 Notch and the awesome power of genetics. Genetics 191: 655–669.

Han, S. M., H. Tsuda, Y. Yang, J. Vibbert, P. Cottee *et al.*, 2012 Secreted VAPB/ALS8 major sperm protein domains modulate mitochondrial localization and morphology via growth cone guidance receptors. Dev. Cell 22: 348–362.

Hardy, J., 2006 A hundred years of Alzheimer's disease research. Neuron 52: 3–13.

Hardy, J., and D. J. Selkoe, 2002 The amyloid hypothesis of Alzheimer's disease: progress and problems on the road to therapeutics. Science 297: 353–356.

Ito, E., K. Oka, R. Etcheberrigaray, T. J. Nelson, D. L. McPhie *et al.*, 1994 Internal Ca2+ mobilization is altered in fibroblasts from patients with Alzheimer disease. Proc. Natl. Acad. Sci. USA 91: 534–538.

Jin, Y., E. Jorgensen, E. Hartwieg, and H. R. Horvitz, 1999 The Caenorhabditis elegans gene unc-25 encodes glutamic acid decarboxylase and is required for synaptic transmission but not synaptic development. J. Neurosci. 19: 539–548.

Johnson, D., E. Allman, and K. Nehrke, 2012 Regulation of acid-base transporters by reactive oxygen species following mitochondrial fragmentation. Am. J. Physiol. Cell Physiol. 302: C1045–C1054.

Kelsh, R., R. You, C. Horzempa, M. Zheng, and P. J. McKeown-Longo, 2014 Regulation of the innate immune response by fibronectin: synergism between the III-1 and EDA domains. PLoS One 9: e102974.

Kim, H., J. T. Pierce-Shimomura, H. J. Oh, B. E. Johnson, M. B. Goodman *et al.*, 2009 The dystrophin complex controls bk channel localization and muscle activity in Caenorhabditis elegans. PLoS Genet. 5: e1000780.

Kipanyula, M. J., L. Contreras, E. Zampese, C. Lazzari, A. K. Wong *et al.*, 2012 Ca2+ dysregulation in neurons from transgenic mice expressing mutant presenilin 2. Aging Cell 11: 885–893.

Kitagawa, N., S. Shimohama, T. Oeda, K. Uemura, R. Kohno *et al.*, 2003 The role of the presenilin-1 homologue gene sel-12 of Caenorhabditis elegans in apoptotic activities. J. Biol. Chem. 278: 12130–12134.

Kovacs, D. M., H. J. Fausett, K. J. Page, T. W. Kim, R. D. Moir *et al.*, 1996 Alzheimer-associated presenilins 1 and 2: neuronal expression in brain and localization to intracellular membranes in mammalian cells. Nat. Med. 2: 224–229.

Lee, R. Y., L. Lobel, M. Hengartner, H. R. Horvitz, and L. Avery, 1997 Mutations in the alpha1 subunit of an L-type voltage-activated Ca2+ channel cause myotonia in Caenorhabditis elegans. EMBO J. 16: 6066–6076.

Leissring, M. A., B. A. Paul, I. Parker, C. W. Cotman, and F. M. LaFerla, 1999 Alzheimer's presenilin-1 mutation potentiates inositol 1,4,5-trisphosphate-mediated calcium signaling in Xenopus oocytes. J. Neurochem. 72: 1061–1068.

Lesne, S., L. Kotilinek, and K. H. Ashe, 2008 Plaque-bearing mice with reduced levels of oligomeric amyloid-beta assemblies have intact memory function. Neuroscience 151: 745–749.

Leuner, K., W. E. Muller, and A. S. Reichert, 2012 From mitochondrial dysfunction to amyloid beta formation: novel insights into the pathogenesis of Alzheimer's disease. Mol. Neurobiol. 46: 186–193.

Levitan, D., and I. Greenwald, 1995 Facilitation of lin-12-mediated signalling by sel-12, a Caenorhabditis elegans S182 Alzheimer's disease gene. Nature 377: 351–354.

Levitan, D., and I. Greenwald, 1998 Effects of SEL-12 presenilin on LIN-12 localization and function in Caenorhabditis elegans. Development 125: 3599–3606.

Li, X., and I. Greenwald, 1997 HOP-1, a Caenorhabditis elegans presenilin, appears to be functionally redundant with SEL-12 presenilin and to facilitate LIN-12 and GLP-1 signaling. Proc. Natl. Acad. Sci. USA 94: 12204–12209.

Liewald, J. F., M. Brauner, G. J. Stephens, M. Bouhours, C. Schultheis *et al.*, 2008 Optogenetic analysis of synaptic function. Nat. Methods 5: 895–902.

Liu, P., Q. Ge, B. Chen, L. Salkoff, M. I. Kotlikoff *et al.*, 2011 Genetic dissection of ion currents underlying all-or-none action potentials in C. elegans body-wall muscle cells. J. Physiol. 589: 101–117.

Lu, Y., S. G. Rolland, and B. Conradt, 2011 A molecular switch that governs mitochondrial fusion and fission mediated by the BCL2-like protein CED-9 of Caenorhabditis elegans. Proc. Natl. Acad. Sci. USA 108: E813–E822.

Mahoney, T. R., S. Luo, E. K. Round, M. Brauner, A. Gottschalk *et al.*, 2008 Intestinal signaling to GABAergic neurons regulates a rhythmic behavior in Caenorhabditis elegans. Proc. Natl. Acad. Sci. USA 105: 16350–16355.

McColl, G., B. R. Roberts, T. L. Pukala, V. B. Kenche, C. M. Roberts *et al.*, 2012 Utility of an improved model of amyloid-beta (Abeta(1)(-)(4)(2)) toxicity in Caenorhabditis elegans for drug screening for Alzheimer's disease. Mol. Neurodegener. 7: 57.

Michalak, M., E. F. Corbett, N. Mesaeli, K. Nakamura, and M. Opas, 1999 Calreticulin: one protein, one gene, many functions. Biochem. J. 344(Pt 2): 281–292.

Moerman, D. G., and A. Fire, 1997 Muscle: structure, function, and development, Chapter 16 in *C. elegans II*, edited by D. L. Riddle, T. Blumenthal, B. J. Meyer, and J. R. Priess. Cold Spring Harbor Laboratory Press, Cold Spring Harbor, NY.

Nordberg, A., 2008 Amyloid plaque imaging in vivo: current achievement and future prospects. Eur. J. Nucl. Med. Mol. Imaging 35(Suppl 1): S46–S50.

Pan, X., J. Liu, T. Nguyen, C. Liu, J. Sun *et al.*, 2013 The physiological role of mitochondrial calcium revealed by mice lacking the mitochondrial calcium uniporter. Nat. Cell Biol. 15: 1464–1472.

Priess, J. R., 2005 Notch signaling in the C. elegans embryo. (June 25, 2005), WormBook, ed. The C. elegans Research Community, WormBook, doi/10.1895/wormbook.1.4.1, http://www.wormbook.org.

Rajaraman, V., and M. Schulder, 1999 Postoperative MRI appearance after transsphenoidal pituitary tumor resection. Surg. Neurol. 52: 592–598, discussion 598–599.

Schon, E. A., and E. Area-Gomez, 2013 Mitochondria-associated ER membranes in Alzheimer disease. Mol. Cell. Neurosci. 55: 26–36.

Sedensky, M. M., J. M. Siefker, and P. G. Morgan, 2001 Model organisms: new insights into ion channel and transporter function. Stomatin homologues interact in Caenorhabditis elegans. Am. J. Physiol. Cell Physiol. 280: C1340–C1348.

Sepulveda-Falla, D., A. Barrera-Ocampo, C. Hagel, A. Korwitz, M. F. Vinueza-Veloz *et al.*, 2014 Familial Alzheimer's disease-associated

presenilin-1 alters cerebellar activity and calcium homeostasis. J. Clin. Invest. 124: 1552–1567.

Sherrington, R., E. I. Rogaev, Y. Liang, E. A. Rogaeva, G. Levesque *et al.*, 1995 Cloning of a gene bearing missense mutations in early-onset familial Alzheimer's disease. Nature 375: 754–760.

Smith, I. F., B. Hitt, K. N. Green, S. Oddo, and F. M. LaFerla, 2005 Enhanced caffeine-induced Ca2+ release in the 3xTg-AD mouse model of Alzheimer's disease. J. Neurochem. 94: 1711–1718.

Spooner, P. M., J. Bonner, A. V. Maricq, G. M. Benian, and K. R. Norman, 2012 Large isoforms of UNC-89 (obscurin) are required for muscle cell architecture and optimal calcium release in Caenorhabditis elegans. PLoS One 7: e40182.

Struhl, G., and I. Greenwald, 1999 Presenilin is required for activity and nuclear access of Notch in Drosophila. Nature 398: 522–525.

Stutzmann, G. E., A. Caccamo, F. M. LaFerla, and I. Parker, 2004 Dysregulated IP3 signaling in cortical neurons of knock-in mice expressing an Alzheimer's-linked mutation in presenilin1 results in exaggerated Ca2+ signals and altered membrane excitability. J. Neurosci. 24: 508–513.

Swerdlow, R. H., J. M. Burns, and S. M. Khan, 2010 The Alzheimer's disease mitochondrial cascade hypothesis. J. Alzheimers Dis. 20(Suppl 2): S265–S279.

Takemura, H., A. R. Hughes, O. Thastrup, and J. W. Putney, Jr., 1989 Activation of calcium entry by the tumor promoter thapsigargin in parotid acinar cells. Evidence that an intracellular calcium pool and not an inositol phosphate regulates calcium fluxes at the plasma membrane. J. Biol. Chem. 264: 12266–12271.

Tedde, A., B. Nacmias, M. Ciantelli, P. Forleo, E. Cellini *et al.*, 2003 Identification of new presenilin gene mutations in early-onset familial Alzheimer disease. Arch. Neurol. 60: 1541–1544.

Terry, R. D., E. Masliah, D. P. Salmon, N. Butters, R. DeTeresa *et al.*, 1991 Physical basis of cognitive alterations in Alzheimer's disease: synapse loss is the major correlate of cognitive impairment. Ann. Neurol. 30: 572–580.

Tu, H., O. Nelson, A. Bezprozvanny, Z. Wang, S. F. Lee *et al.*, 2006 Presenilins form ER Ca2+ leak channels, a function disrupted by familial Alzheimer's disease-linked mutations. Cell 126: 981–993.

Venditti, P., L. Di Stefano, and S. Di Meo, 2013 Mitochondrial metabolism of reactive oxygen species. Mitochondrion 13: 71–82.

Villemagne, V. L., M. T. Fodero-Tavoletti, K. E. Pike, R. Cappai, C. L. Masters *et al.*, 2008 The ART of loss: Abeta imaging in the evaluation of Alzheimer's disease and other dementias. Mol. Neurobiol. 38: 1–15.

Xu, K., N. Tavernarakis, and M. Driscoll, 2001 Necrotic cell death in C. elegans requires the function of calreticulin and regulators of Ca(2+) release from the endoplasmic reticulum. Neuron 31: 957–971.

Xu, S., and A. D. Chisholm, 2014 C. elegans epidermal wounding induces a mitochondrial ROS burst that promotes wound repair. Dev. Cell 31: 48–60.

Xu, S., H. Pi, Y. Chen, N. Zhang, P. Guo *et al.*, 2013 Cadmium induced Drp1-dependent mitochondrial fragmentation by disturbing calcium homeostasis in its hepatotoxicity. Cell Death Dis. 4: e540.

Zampese, E., C. Fasolato, M. J. Kipanyula, M. Bortolozzi, T. Pozzan *et al.*, 2011 Presenilin 2 modulates endoplasmic reticulum (ER)-mitochondria interactions and Ca2+ cross-talk. Proc. Natl. Acad. Sci. USA 108: 2777–2782.

Zhao, Y., S. Araki, J. Wu, T. Teramoto, Y. F. Chang *et al.*, 2011 An expanded palette of genetically encoded Ca(2)(+) indicators. Science 333: 1888–1891.

Communicating editor: M. V. Sundaram

GENETICS

Supporting Information
www.genetics.org/lookup/suppl/doi:10.1534/genetics.115.182808/-/DC1

A γ-Secretase Independent Role for Presenilin in Calcium Homeostasis Impacts Mitochondrial Function and Morphology in *Caenorhabditis elegans*

Shaarika Sarasija and Kenneth R. Norman

DOI: 10.1534/genetics.115.182808

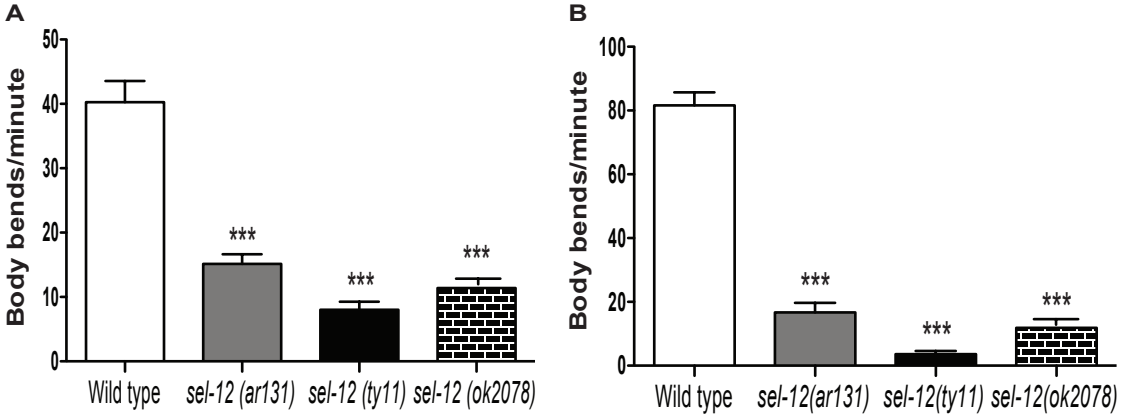

Figure S1. *sel-12* mutants have decreased motility. (A) Crawling assay on NGM plates using wild type and *sel-12* mutants. (B) Swimming assay in M9 using wild type and *sel-12* mutants. n=25 per strain for both assays and data are displayed as mean ± SEM and all comparisons have been made to WT unless otherwise indicated (***p<0.001 using two-way ANOVA).

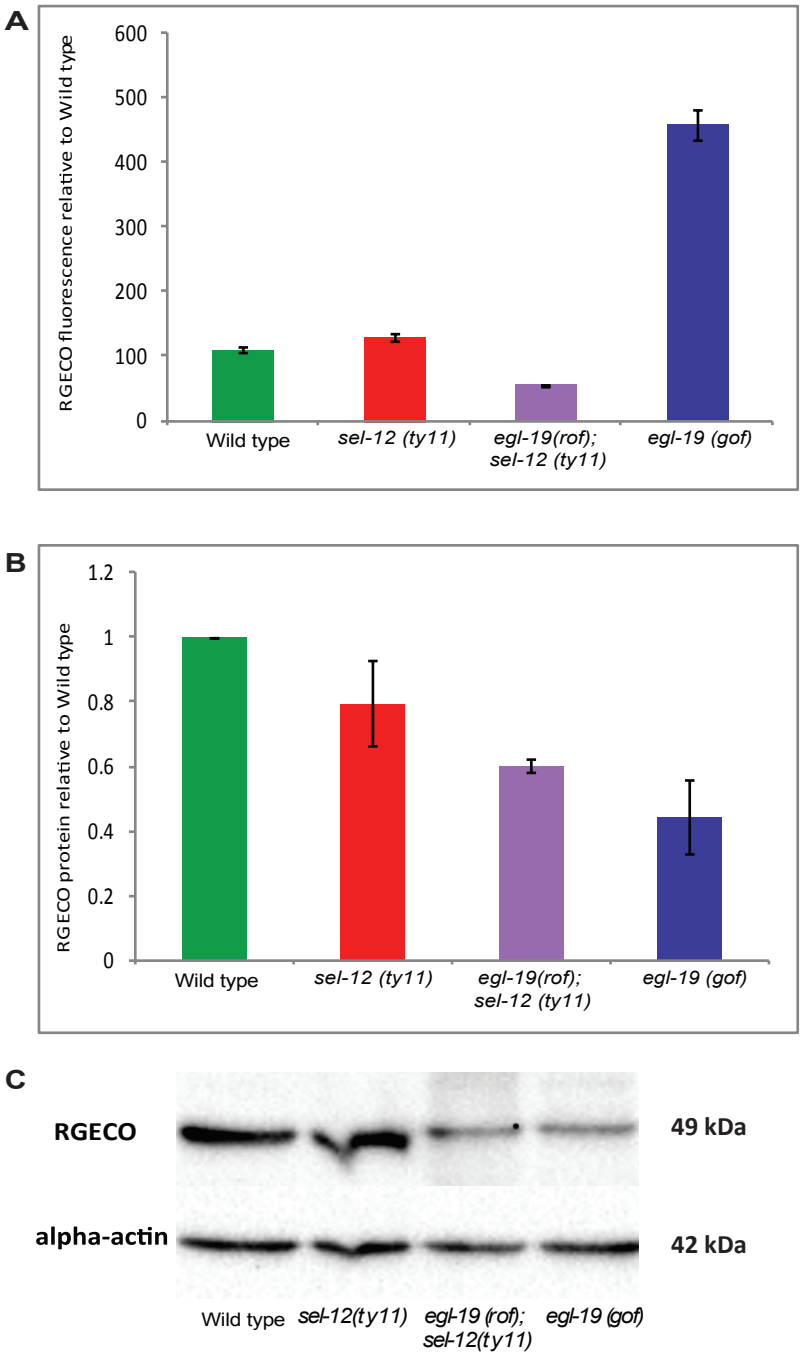

Figure S2. Basal cytoplasmic calcium measurement. (A) Quantification of the relative R-GECO1 fluorescence in each strain with respect to wild type animals (n=50 per strain). (B) Quantification of the relative R-GECO1 protein expression in each strain with respect to wild type animals (average of intensities from 3 western blots). (C) Representative western blot performed for R-GECO1 quantification (alpha-actin used as loading control). Data are displayed as mean ± SEM and all comparisons have been made to WT unless otherwise indicated.

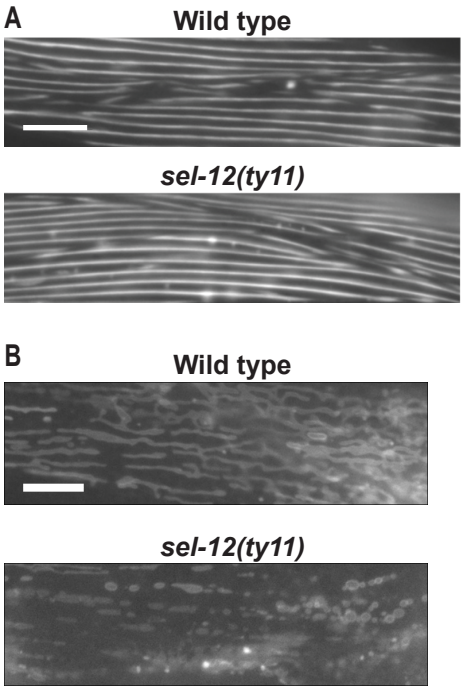

Figure S3. Mitochondrial structural defects in *sel-12* mutants are not caused by muscle structure abnormalities. (A) Representative images of body wall muscle myofilament organization (*stEx30*) in wild type and *sel-12(ty11)* animals. (B) Representative images of body wall muscle mitochondria in wild type and *sel-12(ty11)* animals visualized using a reporter strain that targets mCherry to the outer mitochondrial membrane (*sysIs243*). Scale bar represents 10 μm.

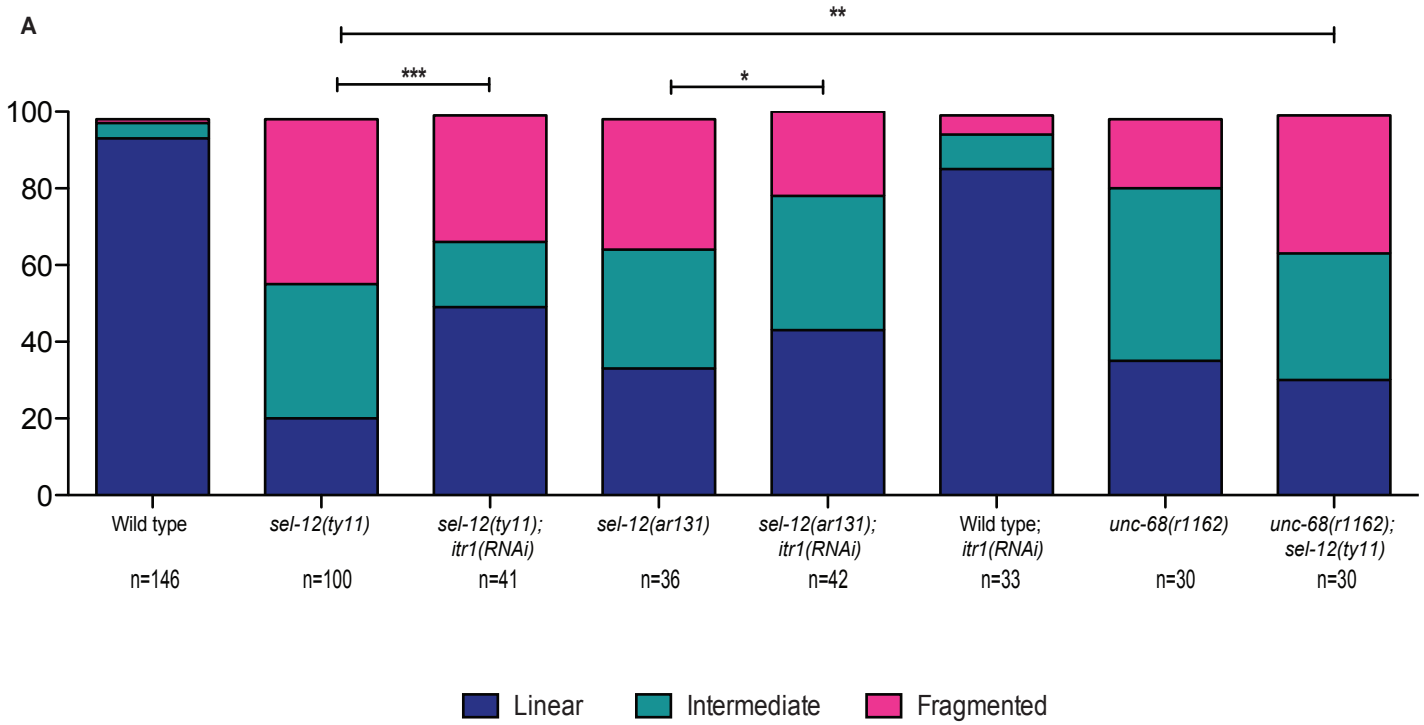

Figure S4. Decreasing ER-mediated calcium release improves mitochondrial structure in *sel-12* mutant. (A) Quantification of body wall muscle mitochondrial morphology in wild type and *sel-12(ty11)* grown on control or *itr-1* RNAi, *unc-68(r1162)*, and *unc-68(r1162)*; *sel-12(ty11)* animals. n = number of animals imaged per genotype, all comparisons have been made to WT unless otherwise indicated and statistical significance was tested using the Chi-square test (*** $p<0.001$, ns not significant).

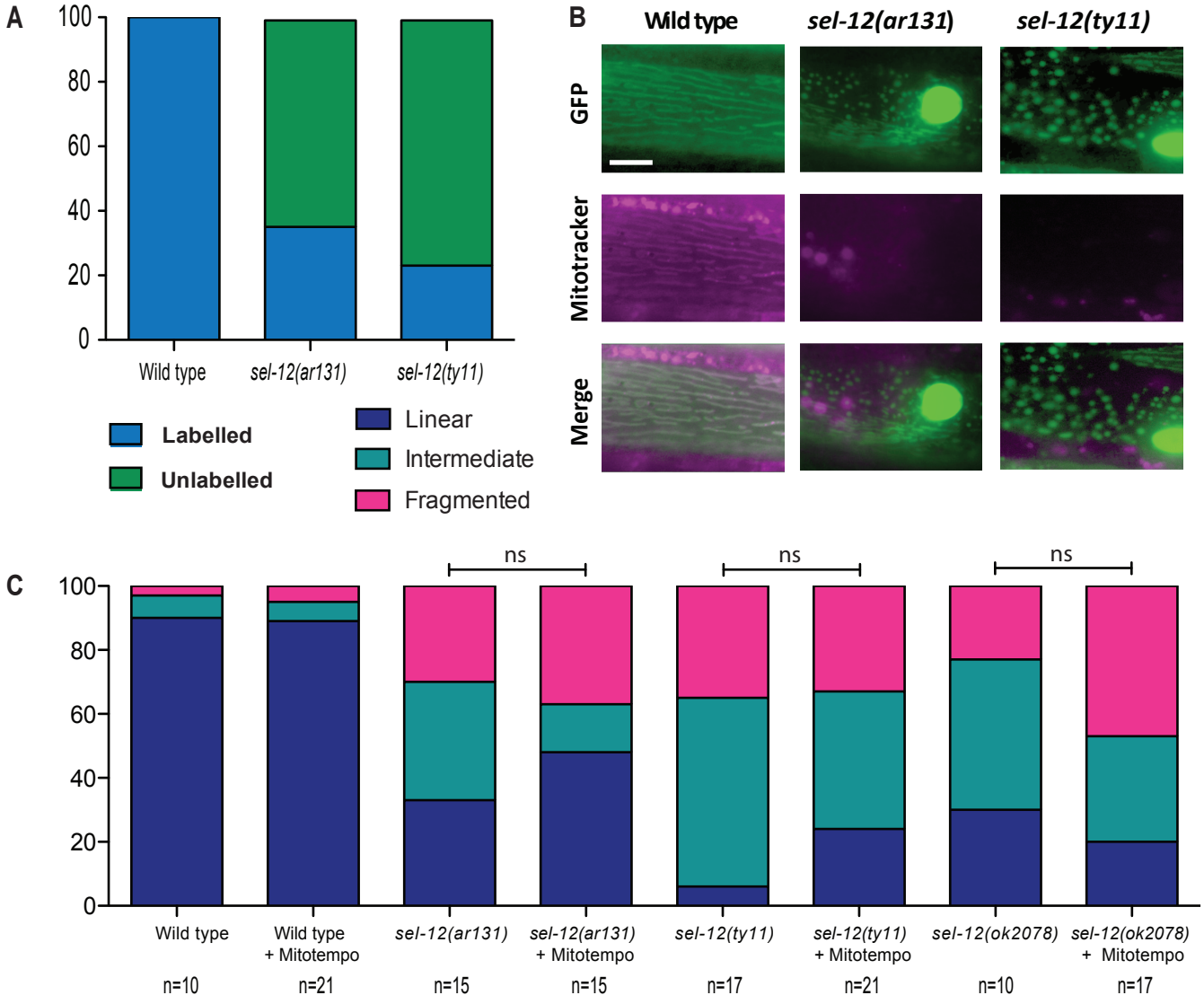

Figure S5. *sel-12* mutants have mitochondrial functional defects. (A) Quantification of body wall muscle mitochondria staining with MitoTracker (labeled [blue] vs. unlabeled [green]) in wild type and *sel-12* animals. (B) Representative images of mitochondrial morphology visualized using GFP (*ccIs4251*) and MitoTracker® Red CMXRos in wild type, *sel-12(ar131)*, and *sel-12(ty11)* animals. Scale bar represents 10 µm. (C) Quantification of body wall muscle mitochondrial morphology in wild type and *sel-12* animals grown on NGM plates containing MitoTempo. n = number of animals imaged per genotype, all comparisons have been made to WT unless otherwise indicated and statistical significance was tested using the Chi-square test (*** $p<0.001$, ns not significant).